



Nitrogen assisted formation of large-area ripples on Ti6Al4V surface by nanosecond pulse laser irradiation

Chao Wang^a, Hu Huang^{a,*}, Yongfeng Qian^a, Zhiyu Zhang^b, Weihai Huang^c, Jiwang Yan^c

^a Key Laboratory of CNC Equipment Reliability, Ministry of Education, School of Mechanical and Aerospace Engineering, Electron Microscopy Center, Jilin University, Changchun, Jilin, 130022, China

^b Key Laboratory of Optical System Advanced Manufacturing Technology, Changchun Institute of Optics, Fine Mechanics and Physics, Chinese Academy of Sciences, Changchun, People's Republic of China

^c Department of Mechanical Engineering, Faculty of Science and Technology, Keio University, Yokohama 223-8522, Japan

ARTICLE INFO

Keywords:

Ti6Al4V
Nanosecond pulse laser
LIPSS
Ripple
Nitrogen

ABSTRACT

Ti6Al4V is one of the most widely used titanium alloys due to its excellent mechanical, physical, and chemical properties. Laser surface texturing is a promising method to endow new functions of material surfaces; however, direct generation of laser-induced periodic surface structure (LIPSS) on the Ti6Al4V surface by nanosecond laser is rarely reported. In this study, by nanosecond laser irradiation in nitrogen atmosphere, the ripples (a typical LIPSS) were directly fabricated on the Ti6Al4V surface. By single-line laser scanning, the effects of laser irradiation parameters including the laser power and repetition frequency on the formation and evolution of the ripples were systematically investigated, followed by optimizing the laser irradiation parameters to achieve the large-area regular and clear ripples with relatively good surface quality as well. Furthermore, by performing contrast experiments in argon atmosphere, the role of nitrogen atmosphere on the formation of ripples was confirmed. Accordingly, formation mechanism of the ripples was discussed. Finally, the effects of the formed ripples on the surface color and wettability were preliminarily characterized to demonstrate the potential applications of surface ripples. This paper provides a nitrogen assisted method to fabricate large-area ripples on the Ti6Al4V surface by nanosecond laser irradiation.

1. Introduction

Taking excellent mechanical, physical, and chemical properties such as high specific strength, low density, excellent characteristics at high temperature as well as good corrosion resistance and biological compatibility, Ti6Al4V has been widely employed in national defense, aerospace, biomedical and other fields [1–3]. However, some shortcomings, such as high friction coefficient, low hardness and wear resistance, limit its industrial applications to some extent [1]. Therefore, surface modification of Ti6Al4V has become an intriguing research topic.

Generally speaking, surface nitriding [4,5] and carburizing [6,7] could improve the surface hardness and wear resistance of titanium alloys. On the other hand, fabrication of micro-/nano-structures on the surface of titanium alloys, i.e. surface texturing, has been confirmed to be a powerful method to enhance or endow the surface functions, such as improving the optical performances [8,9], altering surface wettability

[10,11], and enhancing biological compatibility [12]. Taking advantage of being environmentally friendly and high efficiency, laser-based surface texturing technology has been extensively employed to structure and functionalize the surface of titanium alloys. For example, Rotella et al. [13] utilized a femtosecond laser to prepare the periodic surface structures (i.e., the commonly called laser-induced periodic surface structures, LIPSS) on the Ti6Al4V surface, which improved its adhesion to epoxy resin. Similarly, by using the femtosecond laser, Das et al. [14] prepared LIPSS on titanium film, demonstrating potential applications in high-energy particle physics. Via a picosecond laser, Yu et al. [15] fabricated groove arrays on the Ti6Al4V surface for biomedical application, and the cell proliferation and binding ability to the conjugate were significantly enhanced. When increasing the pulse width to nanosecond, Kosec et al. [16] fabricated microstructures on titanium alloys by using a nanosecond laser, and they further investigated the effect of microstructures on the surface color. To inhibit the growth of bacteria, Patil et al. [17] used the nanosecond laser to form

* Corresponding author.

E-mail address: huanghu@jlu.edu.cn (H. Huang).

<https://doi.org/10.1016/j.precisioneng.2021.09.012>

Received 10 June 2021; Received in revised form 27 August 2021; Accepted 14 September 2021

Available online 21 September 2021

0141-6359/© 2021 Elsevier Inc. All rights reserved.

Table 1
Experimental parameters.

Sample material	Ti6Al4V
Laser wavelength (nm)	1064
Laser pulse width (ns)	7
Laser power P (W)	3.75, 4.04, 4.46, 4.92, 5.21
Laser scanning speed v (mm s^{-1})	10
Pulse overlap rate between two adjacent scanning lines r	88.3%, 76.6%, 53.3%
Laser repetition frequency f (kHz)	300, 400, 500, 600, 700, 800, 900
Atmosphere	Nitrogen, Argon

micro-dimple arrays on the Ti6Al4V surface. By combining nanosecond laser and femtosecond laser, Huerta-Murillo et al. [18] prepared micro-/nano-scale hierarchical structures on the Ti6Al4V surface to achieve super-hydrophobicity.

By analyzing the large number of previous studies working on laser texturing of titanium alloys, ultra-short pulse lasers especially the femtosecond laser, could readily induce the formation of LIPSS on the surface of titanium alloys. Accordingly, for titanium alloys, the research on the formation mechanism [19] and potential applications [20] of LIPSS is mainly based on the femtosecond laser-induced LIPSS. However, for nanosecond laser with a relatively long pulse width, direct generation of LIPSS on the surface of titanium alloys is rarely reported. The publication years of the last two related research articles need to be dated back to 2017 [21] and 2020 [22]. Even so, exploring the possibility to directly create LIPSS on the surface of titanium alloys by nanosecond laser is still quite meaningful and valuable because of its low cost and high efficiency compared to the femtosecond and picosecond lasers [23]. Accordingly, in this study, by attempting nanosecond laser irradiation in nitrogen atmosphere, LIPSS was successfully generated on the Ti6Al4V surface. The effects of laser parameters on the formation and evolution of LIPSS were investigated in detail by single-line laser scanning, followed by optimizing the laser parameters to generate the large-area LIPSS on the Ti6Al4V surface. According to the experimental results and analysis, the formation mechanism of LIPSS was discussed with consideration of the role of nitrogen atmosphere. At last, the effects of generated LIPSS on the surface color and wettability were studied.

2. Materials and experiments

Ti6Al4V samples with dimension of $40 \text{ mm} \times 40 \text{ mm} \times 3 \text{ mm}$ were cut from a thin plate by wire electrical discharge machining (wire-EDM). To remove the oxide layer and surface defects, mechanical grinding and polishing were performed on the polishing machine (Unipol-802, Shenyang Kejing Materials Technology Co., LTD, China) by using 400, 800, 1000, 1200, and 1500 sandpapers in sequence. Then, these samples were cleaned using ethanol. To provide a shielding environment, a specific aluminum box with dimension of $100 \text{ mm} \times 100 \text{ mm} \times 70 \text{ mm}$

was fabricated. Two holes were designed on two adjacent sides of the box, which allowed the shielding gas to pass through. A groove was machined on the cover of the box, and it was further covered by silica glass. When the sample was installed inside the box, the laser could go through the silica glass and reach the sample surface.

The as-prepared samples were irradiated by using the nanosecond fiber laser system (SP-050P-A-EP-Z-F-Y, SPI, UK) with a wavelength of 1064 nm. The laser has a Gaussian beam profile with a circularly polarized state, and a spot diameter of $\sim 43 \mu\text{m}$ at the focused plane. The laser scanning speed and repetition frequency have a similar effect (i.e., the number of pulses per unit length is changed), so the laser scanning speed was fixed to 10 mm s^{-1} through preliminary experiments, and the repetition frequency was changed. For comparison, various laser powers, pulse overlap rates, laser repetition frequencies, and atmospheres were employed. The pulse overlap rates of 88.3%, 76.6%, and 53.3% correspond to the intervals of 5, 10, and $15 \mu\text{m}$ between two adjacent scanning lines, respectively. The detailed experimental parameters mentioned above are listed in Table 1.

After laser irradiation, the resultant surface structures were preliminarily observed by the DSX500 digital microscope (Olympus, Japan), and further observed by using the scanning electron microscope (SEM, JSM-IT500A, JEOL, Japan). The three-dimensional (3D) structures in the irradiated regions were characterized by using the laser scanning confocal microscopy (LSCM, OLS4100, Olympus, Japan). An X-ray diffractometer (XRD, D8 Discover, Bruker, Germany) was employed to characterize the crystal phases before and after laser irradiation in different atmospheres. The structured samples were further immersed in 1 wt% 1H,1H,2H,2H-Perfluorooctyltriethoxysilane-ethanol solution for 1 h and dried at room temperature for 30 min. The wettability of the polished and structured surfaces before and after chemical modification was evaluated by a contact angle measuring instrument (OAS60, NBSI, China), and the droplet volume for measurement was $5 \mu\text{L}$.

3. Results and discussion

3.1. Preliminary selection of laser parameters

Fig. 1 presents the typical optical and SEM morphologies of the single-line scanned region. The used laser power, scanning speed, and repetition frequency were 4.46 W, 10 mm s^{-1} , and 700 kHz, respectively, and the experiments were performed in nitrogen atmosphere. To obtain repeatable results for each experimental condition, single-line scanning was performed along many lines. Here, the single-line scanning means that there is no overlap between two adjacent scanning lines. In Fig. 1(a), the surface shows the color of golden yellow, and the laser scanning traces are visible. In Fig. 1(b) and (c), it is seen that LIPSS (i.e., the ripples) have been formed on Ti6Al4V surface. In addition, some micro-cracks appear around the edges of the scanning line. This kind of ripples has been commonly generated on various materials by

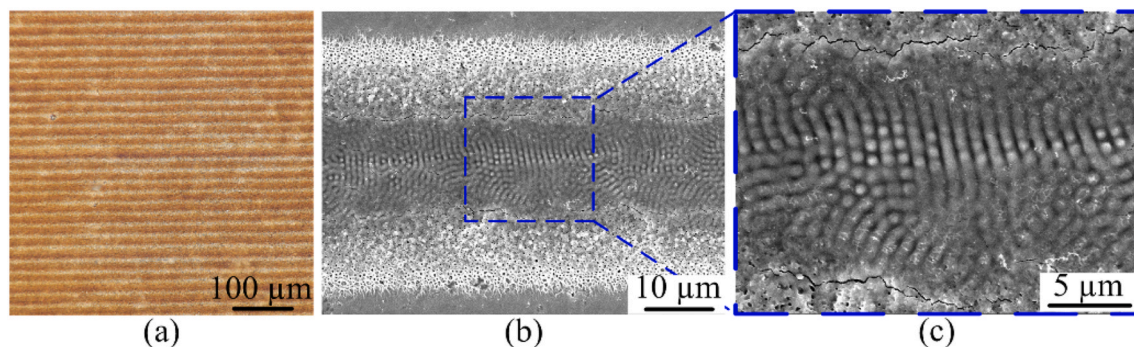


Fig. 1. Typical optical (a) and SEM (b and c) morphologies of the single-line scanned region obtained under the following experimental conditions: $P = 4.46 \text{ W}$, $v = 10 \text{ mm s}^{-1}$, $f = 700 \text{ kHz}$, and nitrogen atmosphere.

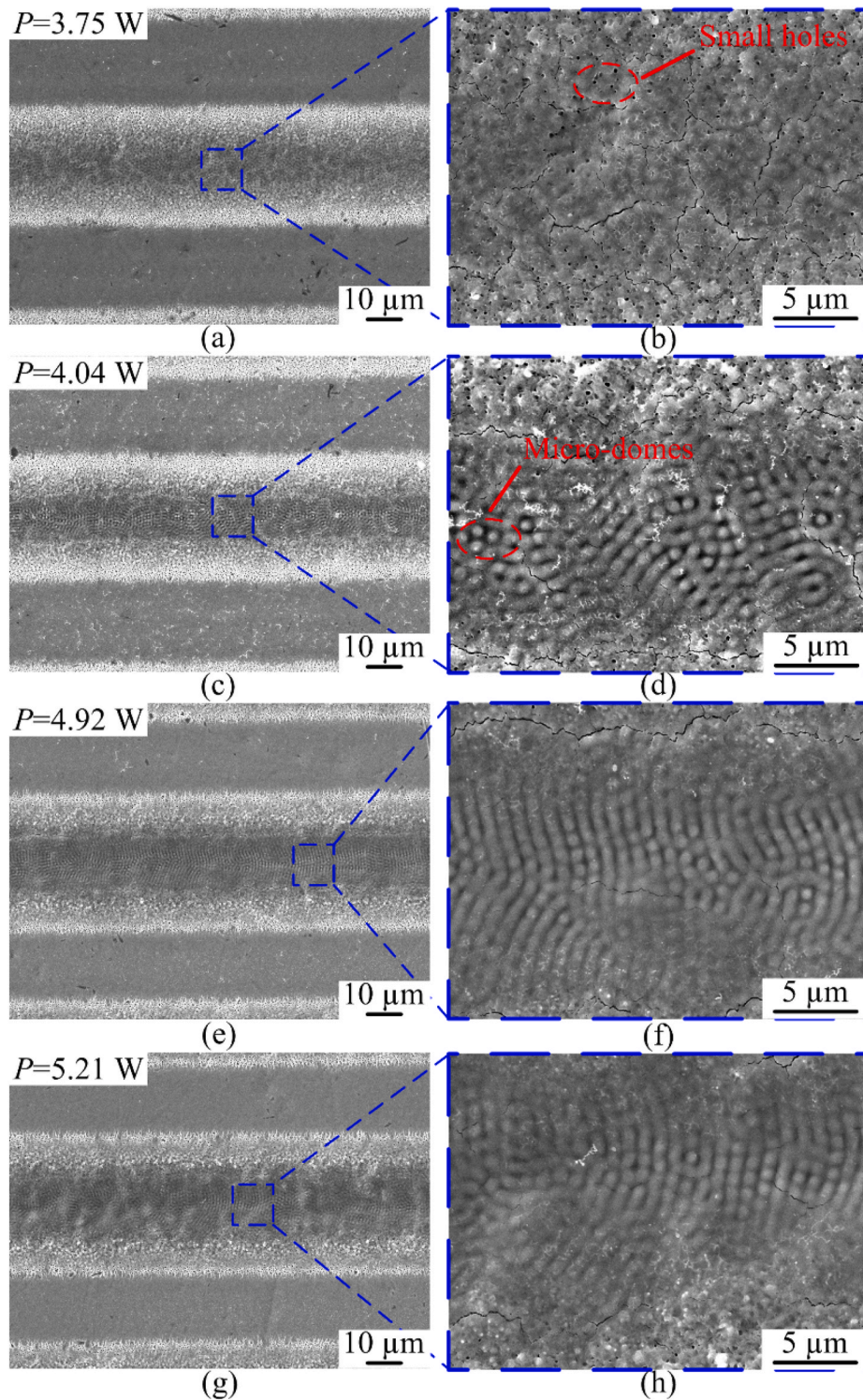


Fig. 2. SEM morphologies of the single-line scanned regions obtained under different laser powers in nitrogen atmosphere ($f = 700 \text{ kHz}$, $v = 10 \text{ mm s}^{-1}$): (a) 3.75 W, (c) 4.04 W, (e) 4.92 W, and (g) 5.21 W. (b), (d), (f) and (h) are the local enlarged images, respectively.

using the femtosecond and picosecond pulse lasers [24–27], but it is rarely reported by using the nanosecond pulse laser.

To investigate the effects of laser irradiation parameters on the formation of ripples and accordingly explore its formation mechanism, single-line laser scanning was further performed under various laser powers and repetition frequencies. Fig. 2 shows the SEM morphologies of the single-line scanned regions obtained under different laser powers. The scanning speed and repetition frequency were kept to be 10 mm s^{-1}

and 700 kHz , respectively. As shown in Fig. 2(a) and (b), when the laser power is 3.75 W, no ripples are generated in the irradiated region; around the central zone, there are many small holes and tiny cracks distributed, and some local bulges appear, showing the tendency to evolve into the ripples. When the laser power increases to 4.04 W, micro-domes appear around the central zone (Fig. 2(d)), and some of them have self-assembled to form the rudiment of ripples but with irregular directions. As shown in Fig. 1(c), when the laser power is 4.46 W,

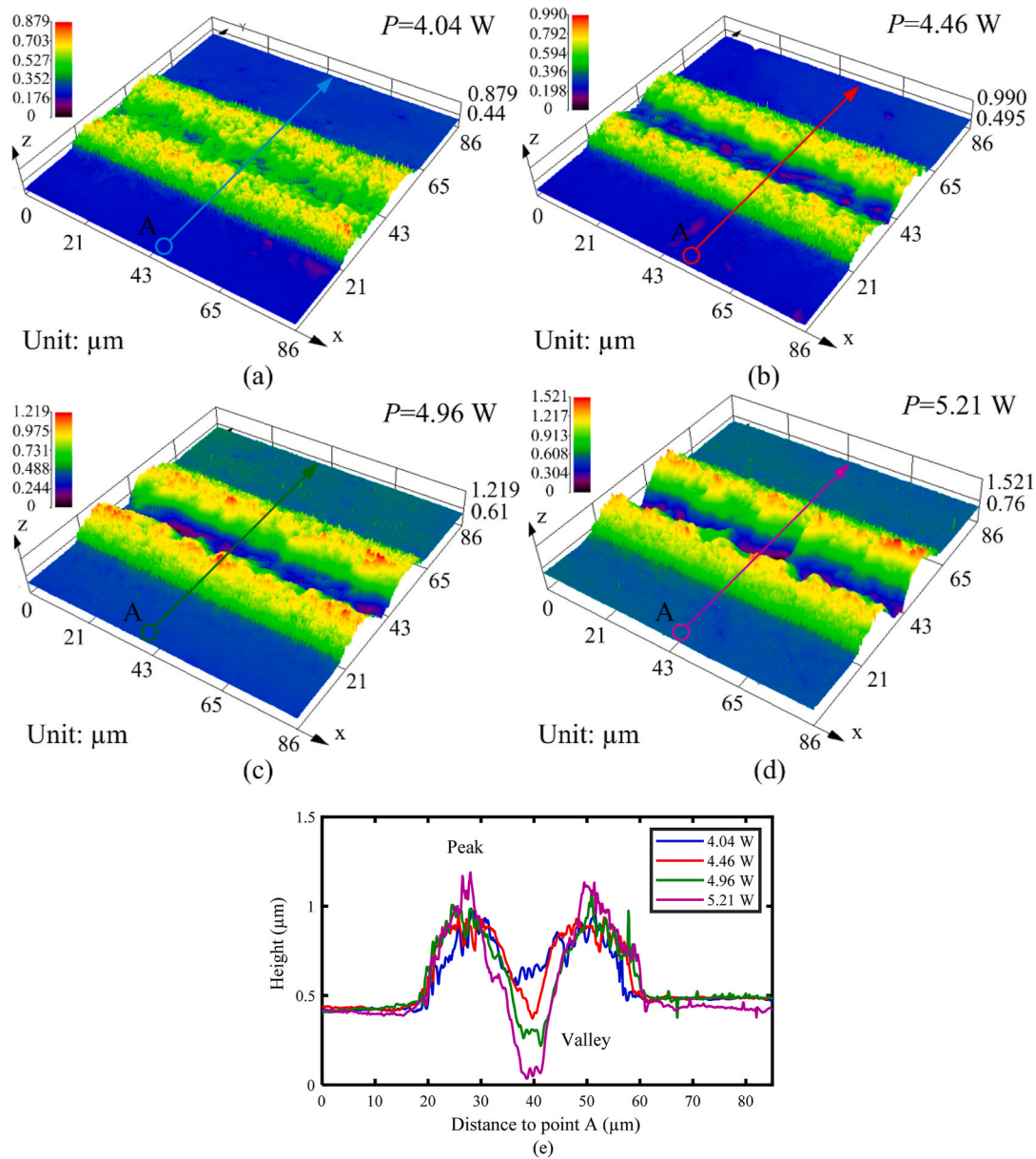


Fig. 3. 3D topographies of the single-line scanned regions obtained under different laser powers in nitrogen atmosphere ($f = 700$ kHz, $v = 10$ mm s^{-1}): (a) 4.04 W, (b) 4.46 W, (c) 4.92 W, and (d) 5.21 W. (e) Profiles of the cross-sections marked in Fig. 3(a)–3(d).

relatively regular ripples have been formed around the central zone. Further increasing the laser power to 4.92 and 5.21 W, the ripples become twisty and shallow, as shown in Fig. 2(e)–2(h). In addition, for all the employed laser powers, micro-cracks could be observed in the irradiated regions.

Fig. 3 presents the 3D topographies of the single-line scanned regions obtained under various laser powers. The other parameters are the same to those in Fig. 2. Distinct valleys and peaks are observed in each laser scanning trace. Due to the complex laser-material interaction, the molten materials around the center of the scanning line are extruded and then re-solidified on both sides, forming the valley and peak at the center and side of the laser scanning trace, respectively. Fig. 3(e) presents the profiles of the cross-sections marked in Fig. 3(a)–3(d). With increase in laser power, the height of the peak and the depth of the valley tend to increase, and these two parameters significantly affect the final quality of laser irradiated surface. Therefore, for fabricating large-area ripples, the laser irradiation parameters should be optimized. According to the comparative results in Figs. 1–3, the laser power was

preliminarily selected as 4.46 W. Under this power, the ripples formed on the Ti6Al4V surface are clear and regular, and the influence of peaks and valleys on the surface quality is also relatively weak.

The laser scanning speed and power were kept to be 10 mm s^{-1} and 4.46 W, respectively. As shown in Fig. 4(a) and (b), when the repetition frequency is lower than 400 kHz, no ripples are generated in the irradiated region. When the frequency is in the range of 500–800 kHz as shown in Fig. 4(c)–4(h), distinct ripples are formed on the Ti6Al4V surface, accompanied with some micro-cracks in the central region. At 500 kHz, the distribution of micro-cracks is disordered; at 600 kHz, the micro-cracks are mainly distributed near the center. Compared to the morphology obtained at 700 kHz (Fig. 1(c)), although more micro-cracks are generated in the irradiated region obtained at 600 kHz, the formed ripples are clearer and more regular. Further increasing the frequency to 800 kHz, the ripples become disordered and micro-domes appear again. Accordingly, the ripples obtained at frequencies of 500–800 kHz were further characterized by using the laser scanning confocal microscopy. Fig. 5(a) presents a typical optical image obtained

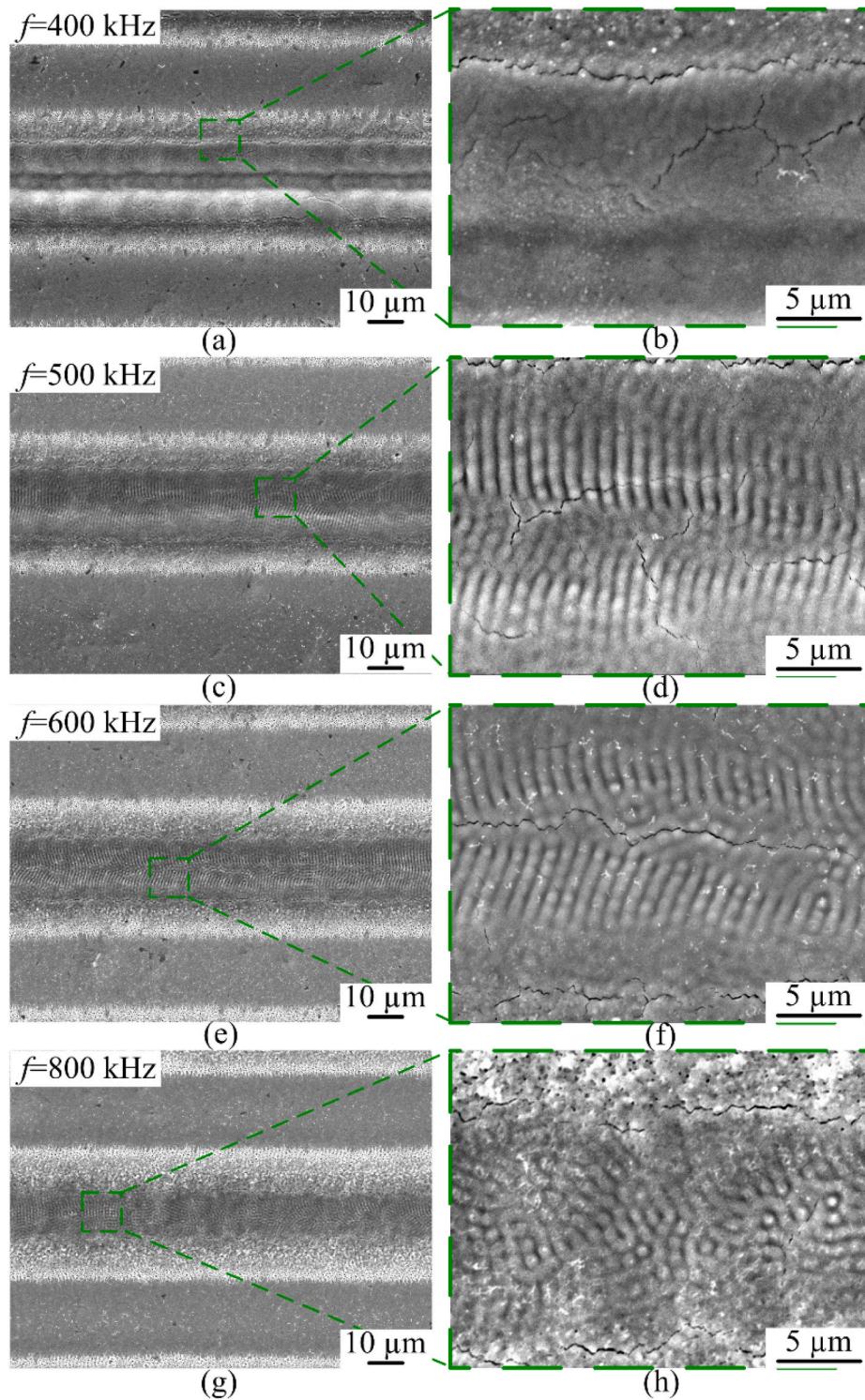


Fig. 4. SEM morphologies of the single-line scanned regions obtained under different repetition frequencies in nitrogen atmosphere ($P = 4.46 \text{ W}$, $v = 10 \text{ mm s}^{-1}$): (a) 400 kHz, (c) 500 kHz, (e) 600 kHz, and (g) 800 kHz. (b), (d), (f), and (h) are the local enlarged images, respectively.

at 600 kHz, and regular ripples are clearly observed, agreeing well with the SEM result. Fig. 5(b) illustrates the profile of the marked line in Fig. 5 (a), from which the period of the ripples could be easily obtained. Fig. 5 (c) presents the statistical results of the period varying with frequency. It is noted that the period of ripples obtained at different frequencies remains at about $0.98 \mu\text{m}$, being almost independent of the repetition frequency.

When the laser repetition frequency changes, two main factors would

cause the experiment results to change. One is the pulse energy, and another is the pulse overlap rate along single scanning line. The pulse energy E can be expressed as

$$E = \frac{P}{f} \quad (1)$$

where P is the average laser power. When the average laser power keeps constant, the pulse energy decreases with increase in repetition

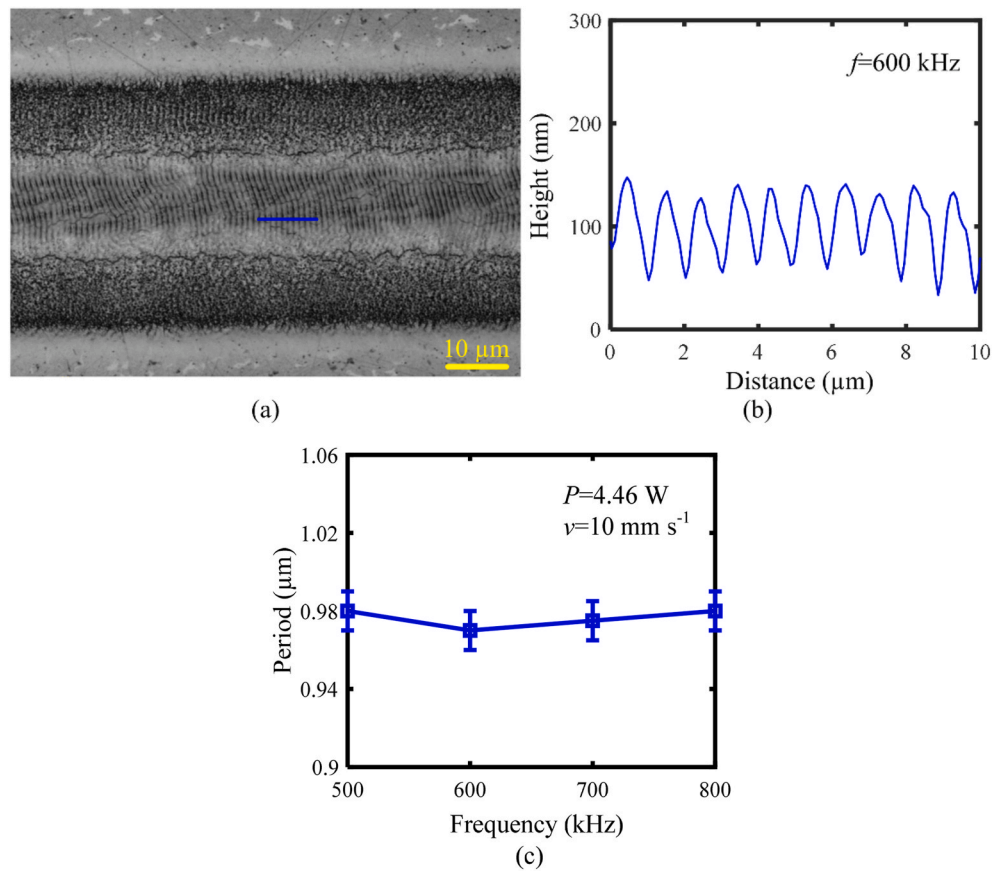


Fig. 5. (a) The optical image obtained at 600 kHz ($P = 4.46$ W, $v = 10$ mm s⁻¹, nitrogen atmosphere), and (b) the profile of the marked line in (a). (c) shows the statistical results of the period varying with the repetition frequency.

frequency, resulting in the change in morphology.

The overlap rate S between two adjacent laser pulses along single scanning line can be calculated by the following formula [28].

$$S = 1 - \frac{v}{2Rf} \quad (2)$$

where R is the radius of laser beam. The calculation results show that under the employed laser repetition frequency, all the corresponding overlap rates are higher than 99%, indicating that the laser overlap rate S during single-line scanning would have very slight effect on the experimental results. According to these comparative results obtained under the laser power of 4.46 W, the repetition frequency of 600 kHz is selected for achieving well-organized ripples during single-line scanning.

3.2. Final optimization of laser parameters

According to the above results obtained by single-line scanning, the laser power and repetition frequency for large-area fabrication of ripples are preliminarily selected as 4.46 W and 600 kHz, respectively. For multi-line scanning, another parameter, i.e. the pulse overlap rate between two adjacent scanning lines will also significantly affect the final surface microstructures. Therefore, the preliminarily selected laser parameters by single-line scanning are further confirmed by multi-line scanning with a given overlap rate of 76.6% between two adjacent scanning lines. In this process, both the morphology of ripples and the final surface quality are considered. The surface roughness parameters S_a and S_z are used to evaluate the surface quality. Fig. 6 shows the SEM morphologies of the multi-line scanned regions obtained under different repetition frequencies. When the frequency is 500 kHz, clear ripples

have been generated on the scanned regions (Fig. 6(a)). However, evident laser scanning traces with grooves and bulges interlaced are observed, and some relatively big cracks appear. As shown in Fig. 6(b), when the frequency increases to 600 kHz, the surface becomes slightly flat with reduced cracks, and the ripples are relatively regular. However, upon the ripples, there is a layer of flocculent nanostructure, probably due to the re-deposition of vaporized materials [29]. As shown in Fig. 6(c) and (d), when the frequency is 700 kHz or 800 kHz, the surface morphologies being similar to that obtained at 600 kHz can be obtained, and furthermore, the resultant surfaces are much cleaner with fewer cracks. When carefully comparing Fig. 6(c)(3) with Fig. 6(d)(3), it is seen that in the interactive region between two adjacent scanning lines, the ripples are more closely connected at 700 kHz.

Fig. 7 presents the 3D topographies obtained under different frequencies. The laser repetition frequencies of Fig. 7(a), (b), (c), and (d) are 500 kHz, 600 kHz, 700 kHz, and 800 kHz, respectively. The valleys and peaks formed by laser irradiation are alternately distributed on the Ti6Al4V surface. When increasing the frequency, both the S_a and S_z tend to decrease slightly, demonstrating that the surface quality is gradually improved. With consideration of both the morphology of ripples and the final surface quality in Figs. 6 and 7, the laser repetition frequency for fabricating the large-area ripples is finally selected to be 700 kHz.

Then, according to the results obtained by single-line scanning, multi-line scanning experiments were further carried out under laser powers of about 4.46 W with other laser parameters fixed. Fig. 8 shows the corresponding SEM morphologies and 3D topographies. In Fig. 8(a), when the power is 4.04 W, the cracks are mainly distributed at the junction of two laser scanning lines and extend locally to the central region. In Fig. 6(c), when the power is 4.46 W, the distribution of surface cracks is similar to that obtained under 4.04 W, but the number of crack propagation decreases. In Fig. 8(b), when the power is 4.92 W, a layer of

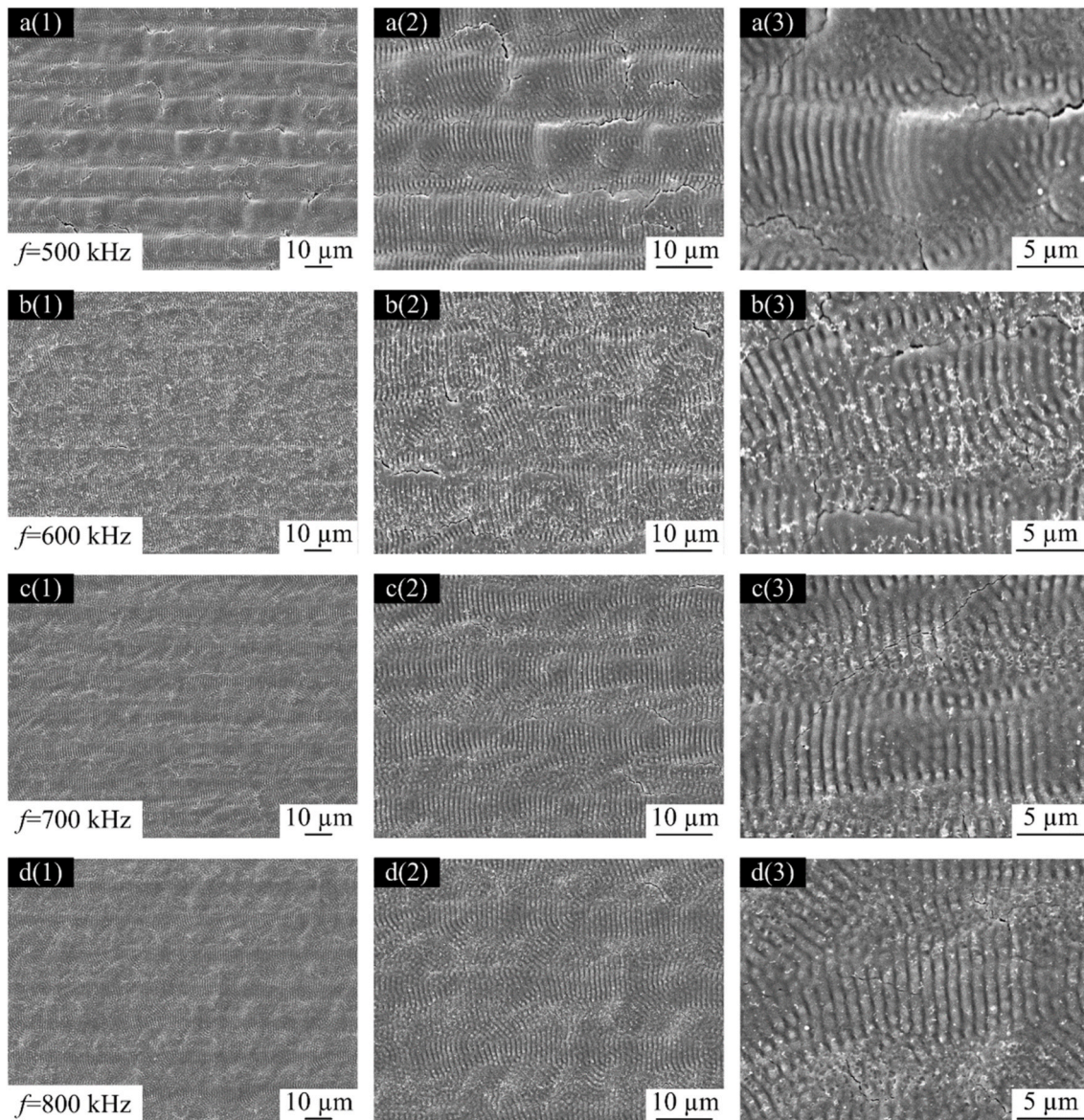


Fig. 6. SEM morphologies of the multi-line scanned regions obtained under different frequencies in nitrogen atmosphere ($P = 4.46 \text{ W}$, $v = 10 \text{ mm s}^{-1}$): (a) 500 kHz, (b) 600 kHz, (c) 700 kHz, and (d) 800 kHz. Numbers (1, 2, 3) in parentheses after letters mean that those three images are obtained with different magnifications.

flocules is formed on the surface, which significantly affects the surface quality. Fig. 8(c) and (d) show the 3D topographies of the multi-line scanned regions. With increase in laser power, both the S_a and S_z slightly increase, indicating that the surface quality is deteriorated. Comprehensively considering the morphology of ripples and surface quality, the laser power is selected as 4.46 W.

For multi-line laser scanning, the pulse overlap rate is another key parameter for fabrication of large-area ripples. In the above multi-line scanning experiments, the used pulse overlap rate was 76.6%. For comparison, Fig. 9(a) and (b) present the SEM morphologies obtained another two pulse overlap rates, 83.3% and 53.5%, respectively. As shown in Fig. 9(a), when the pulse overlap rate is 83.3%, the ripples are surrounded by pits and scattered cracks which deteriorate the quality of the ripples and the irradiated surface. This is due to that when increasing the pulse overlap rate, the formed ripples in the preceding laser scanning line would still in the irradiation region of the next laser scanning line, and thus they would be affected by the next laser scanning line, leading to deteriorated ripples and surface quality. In Fig. 9(b), when the pulse overlap rate is decreased to 53.5%, the ripples are formed only in the center area of each scanning line, and furthermore, cracks still appear in

the junction of the two scanning lines. In this case, the laser energy in the junction is insufficient to achieve the critical condition for generating the ripples.

Finally, according to the above comparative experiments and results, the preferred laser parameters for fabrication of large-area ripples on Ti6Al4V surface are as follows: $v = 10 \text{ mm s}^{-1}$, $P = 4.46 \text{ W}$, $f = 700 \text{ kHz}$, and $r = 76.6\%$. With these parameters, the formed large-area ripples would be regular and clear as shown in Fig. 6(c), and the surface quality of laser irradiated region is better as well.

3.3. Laser irradiation in argon atmosphere

All the above experiments were performed in nitrogen atmosphere. To explore the effects of irradiation atmosphere, multi-line scanning of Ti6Al4V surface was also performed in argon atmosphere under the preferred laser parameters. After many attempts with different laser powers, no periodic ripples are observed in the irradiated regions. Fig. 10 gives two examples obtained under 6.07 W and 12.00 W. Instead of the ripples, the hexagonal structures with distinct boundary are observed, and furthermore, the needle structures exist in the interior of

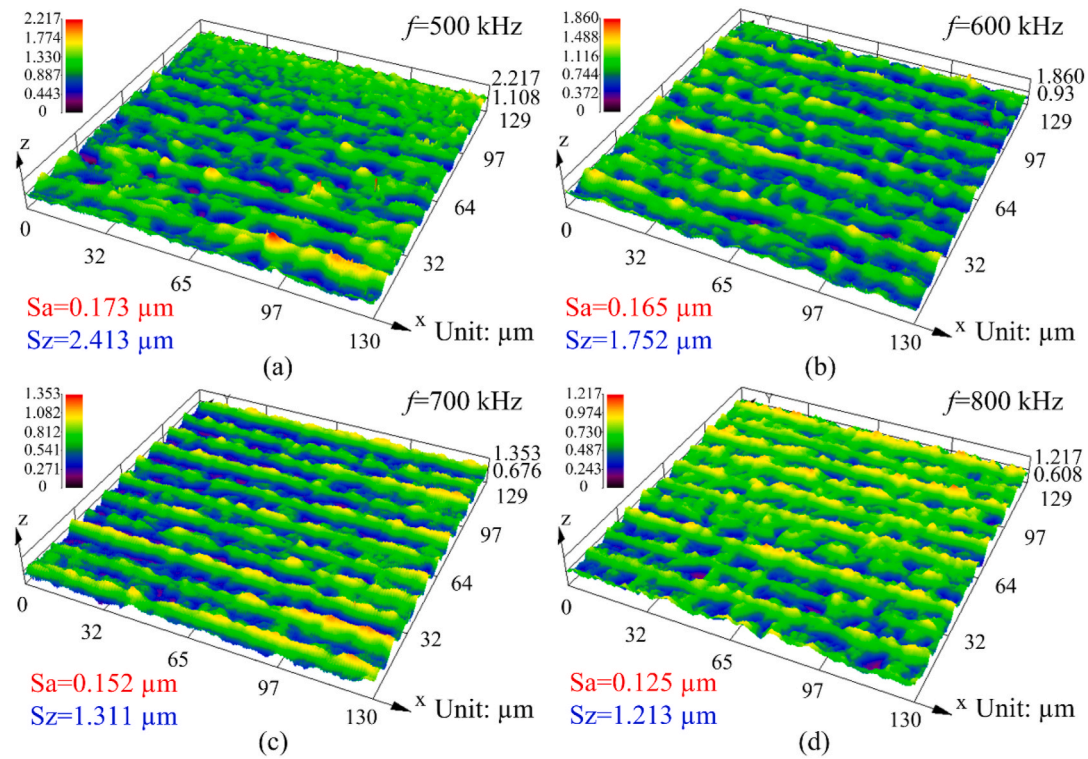


Fig. 7. 3D topographies of the multi-line scanned regions obtained under different frequencies in nitrogen atmosphere ($P = 4.46$ W, $v = 10$ mm s⁻¹): (a) 500 kHz, (b) 600 kHz, (c) 700 kHz, and (d) 800 kHz. Sa and Sz are included in each figure.

the hexagonal structure. With increase in the laser power from 6.07 W to 12.00 W, these two kinds of structures become evident and clear. By comparing the observed structures with some previous literatures, they are very similar to the surface characteristics after selective laser melting [30,31]. Ti6Al4V is a typical double-phase ($\alpha+\beta$) titanium alloy. The β -phase could be transformed into acicular martensite α' due to the high temperature gradient during laser irradiation, and the cyclic thermal effect and rapid cooling rate lead to this regular hexagonal microstructure consisting of prior β columnar grains filled with acicular martensite α' [30–32].

4. Formation mechanism of the LIPSS

Various LIPSSs have been extensively reported in many previous studies [33–35], especially by ultra-short pulse laser irradiation such as picosecond and femtosecond laser irradiation [36,37]. Also, the formation mechanisms of LIPSSs have been investigated for many years, and a series of models have been proposed, for example, the scattering wave model, residual radiation model, capillary wave model, and interference model between incident light and surface plasmon polariton (SPP) [38–42]. Although there is no unified model, the interference model is preferred by many scholars [43]. According to the relationship between the period Λ and wavelength λ , LIPSSs could be further divided into two categories, the low spatial frequency LIPSS (LSFL) with a period being approximately equal to the wavelength length ($\Lambda \approx \lambda$), and the high spatial frequency LIPSS (HSFL) with a period being much smaller than the wavelength ($\Lambda \ll \lambda$) [44,45]. HSFL is a typical phenomenon for ultra-short pulse laser irradiation of materials. But for the nanosecond laser with a relatively long pulse width, the formation of regular LIPSS, especially the preparation of large-area LIPSS, is relatively difficult, due to the non-negligible thermal effect [34,46]. In this study, by nanosecond laser irradiation in nitrogen atmosphere, LSFL has been produced on the Ti6Al4V surface.

4.1. Orientation of ripples

As shown in Fig. 1, it is obvious that the main orientation of the ripples is perpendicular to the laser scanning direction. However, it becomes disorder in some irradiated regions as shown in Fig. 1(c). The possible reasons leading to the disorder are included as follows. Firstly, the defects on the original Ti6Al4V surface would lead to the inhomogeneous absorption of laser energy. Secondly, the micro-cracks induced by laser irradiation would affect the propagation of ripples. As shown in Fig. 6, the orientation of ripples has changed around the cracks. Thirdly, Ti6Al4V has remarkable grain boundaries as shown in Fig. 10, and the laser absorption in these grain boundaries would be also different from the interior of grains. Therefore, the grain boundaries may also affect the orientation of ripples.

4.2. Spatial period of ripples

The spatial period of ripples is mainly determined by the initial ripples [43]. In the irradiated region, the molten layer is formed due to the rapid rise in temperature of the Ti6Al4V surface. At high temperature, the molten layer readily reacts with the surrounding nitrogen, resulting in the formation of TiN. This could be confirmed by the XRD patterns shown in Fig. 11. While, for laser irradiated surface in argon atmosphere, the XRD pattern is very similar to that of the original surface, being without the TiN phase. As laser irradiation in argon atmosphere does not induce the generation of ripples, the role of TiN on the formation of ripples is confirmed.

With consideration of the interference between SPP and laser as well as the subsequent coupling and positive feedback phenomena, the initial ripples are considered to be formed in the molten layer composed of TiN, and the period Λ can be given as [39,47].

$$\Lambda = \frac{\lambda}{\frac{\lambda}{\lambda_s} \pm \sin \theta} \quad (3)$$

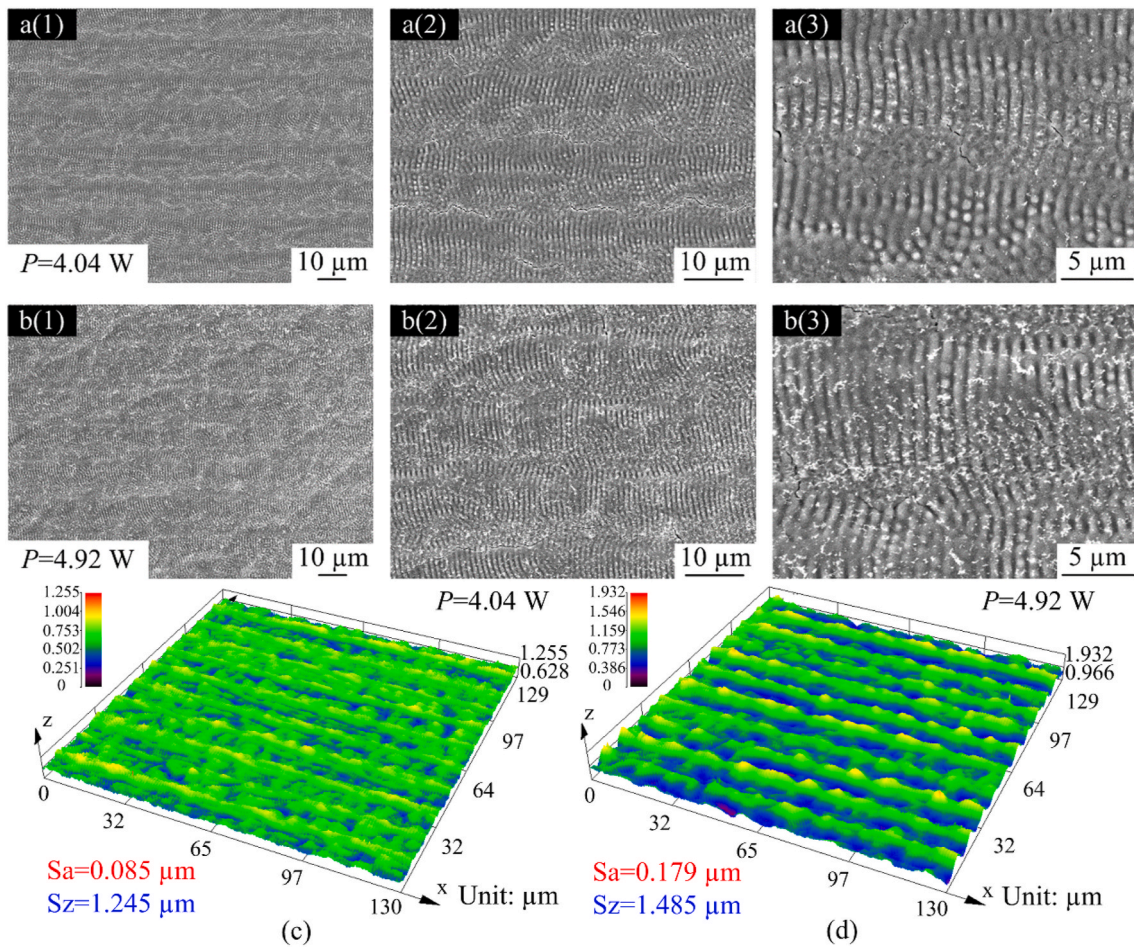


Fig. 8. SEM morphologies of the multi-line scanned regions obtained under different power in nitrogen atmosphere ($f = 700$ kHz, $v = 10$ mm s⁻¹): (a) 4.04 W, and (b) 4.92 W. Numbers (1, 2, 3) in parentheses after letters mean that those three images are obtained with different magnifications. (c) and (d) show the corresponding 3D topographies of the multi-line scanned regions, and S_a and S_z are included in each figure.

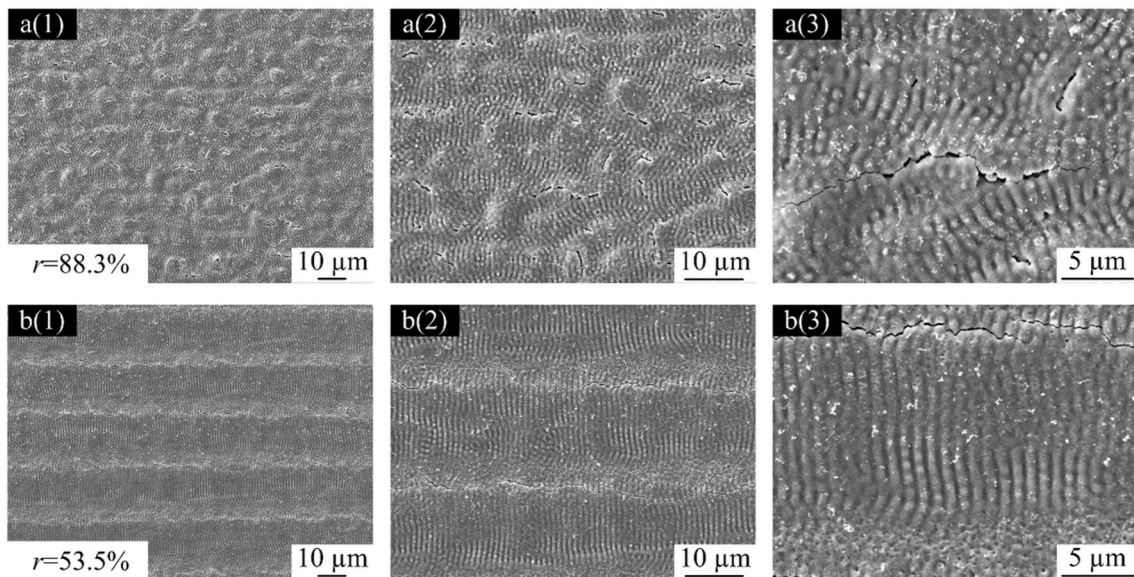


Fig. 9. SEM morphologies of the multi-line scanned regions obtained under different pulse overlap rates in nitrogen atmosphere ($v = 10$ mm s⁻¹, $P = 4.46$ W, $f = 700$ kHz): (a) $r = 88.3\%$, (b) $r = 53.5\%$. Numbers (1, 2, 3) in parentheses after letters mean that those three images are obtained with different magnifications.

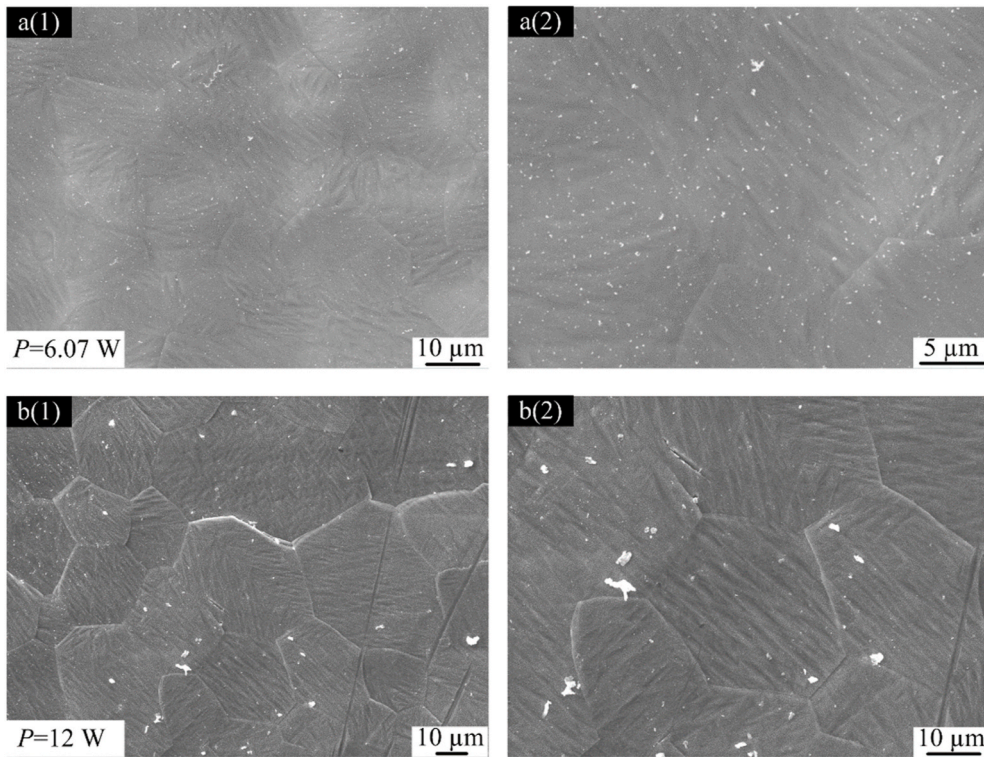


Fig. 10. SEM morphologies of the multi-line scanned regions obtained under different laser powers in argon atmosphere ($v = 10 \text{ mm s}^{-1}$, $f = 700 \text{ kHz}$, $r = 76.6\%$): (a) $P = 6.07 \text{ W}$, and (b) $P = 12.00 \text{ W}$. The images on the right are enlarged images of the left one.

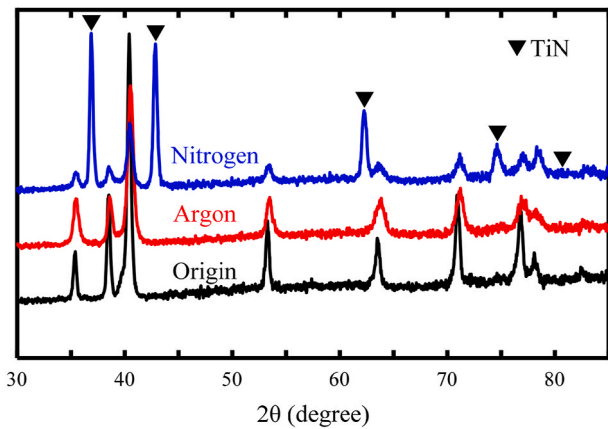


Fig. 11. XRD patterns of original Ti6Al4V surface and the surfaces after laser irradiation in argon and nitrogen atmospheres.

where λ is the wavelength of laser, λ_s is the SPP period, and θ is the incident angle of laser. As Ti6Al4V is not perfect medium, the excitation of SPP on particular interface has to satisfy the condition in Eq. (4) [44, 47].

$$\epsilon'_1 \times \epsilon'_2 + \epsilon''_1 \times \epsilon''_2 < 0 \tag{4}$$

where ϵ'_1 and ϵ''_1 are the real and imaginary parts of the dielectric function for nitrogen, ϵ'_2 and ϵ''_2 are the real and imaginary parts of the dielectric function for molten layer. The SPP period can be calculated by the following equations [44,47].

$$\lambda_s = \frac{2\lambda}{L} \tag{5}$$

$$L = \sqrt{2(L_1^2 + L_2^2)^{\frac{1}{2}} + 2L_1}$$

$$L_0 = \left[(\epsilon'_1 + \epsilon'_2)^2 + \epsilon''_1 + \epsilon''_2 \right]^{-1}$$

$$L_1 = (\epsilon'_1 \epsilon'_2 - \epsilon''_1 \epsilon''_2)(\epsilon'_1 + \epsilon'_2)L_0 + (\epsilon''_1 \epsilon'_2 + \epsilon'_1 \epsilon''_2)(\epsilon''_1 + \epsilon''_2)L_0$$

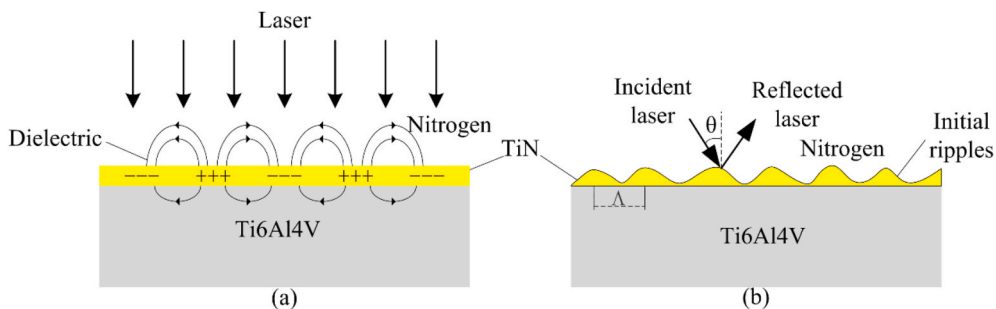


Fig. 12. Schematic diagram illustrating the formation of ripples: (a) interference model and (b) grating coupled model.

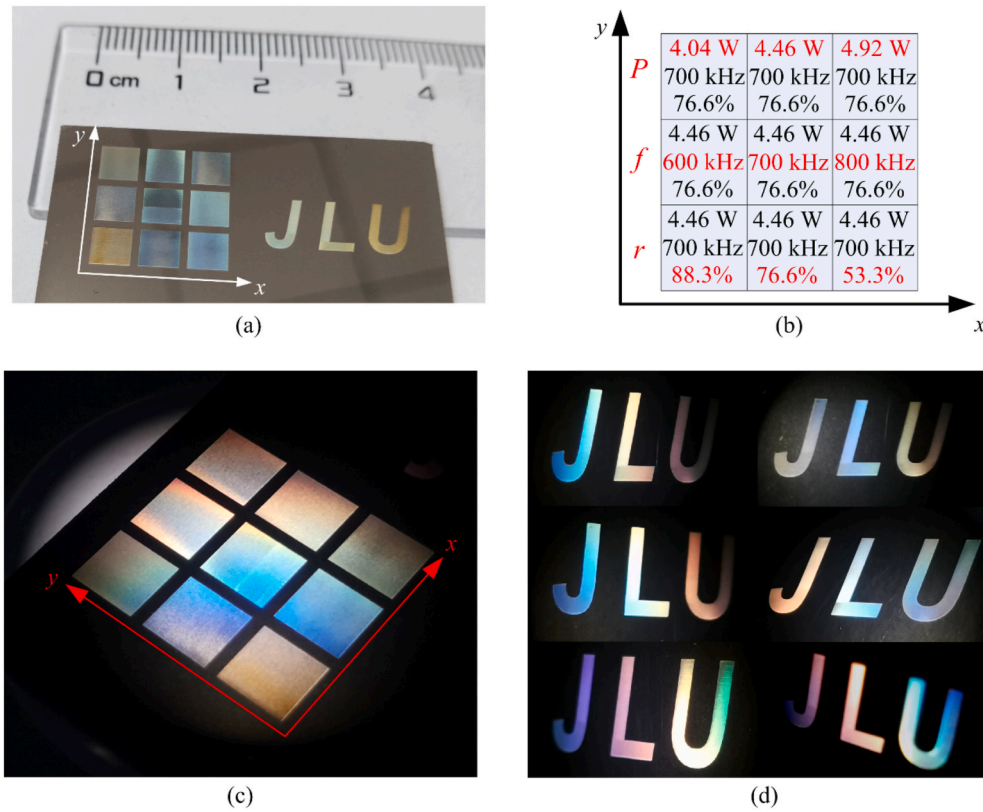


Fig. 13. (a) Optical images of the sample after laser irradiation captured in natural light, and (b) the corresponding laser parameters. (c) shows the optical images “nine-squares” captured in the relatively dark environment with a vertical light source, and (d) shows the color change of “JLU” when changing the shooting angle. (For interpretation of the references to color in this figure legend, the reader is referred to the Web version of this article.)

$$L_2 = (\epsilon_1''\epsilon_2' + \epsilon_1'\epsilon_2'')(\epsilon_1' + \epsilon_2')L_0 - (\epsilon_1'\epsilon_2' - \epsilon_1''\epsilon_2'')(\epsilon_1'' + \epsilon_2'')L_0$$

The dielectric constants of the TiN and nitrogen are $-15.018 + 20.954i$ and 1 , respectively [48], which can excite SPP at the interface of the molten layer and nitrogen. The period of initial ripples obtained by the above formula is about $1.03 \mu\text{m}$ (0.97λ), which is close to the experimentally measured period of about $0.98 \mu\text{m}$ as shown in Fig. 5(c).

The slight difference could be attributed to the feedback mechanism between pulses as well as the change of instantaneous dielectric constant [49].

4.3. Formation mechanism

Due to some irregular defects and impurities on the Ti6Al4V surface,

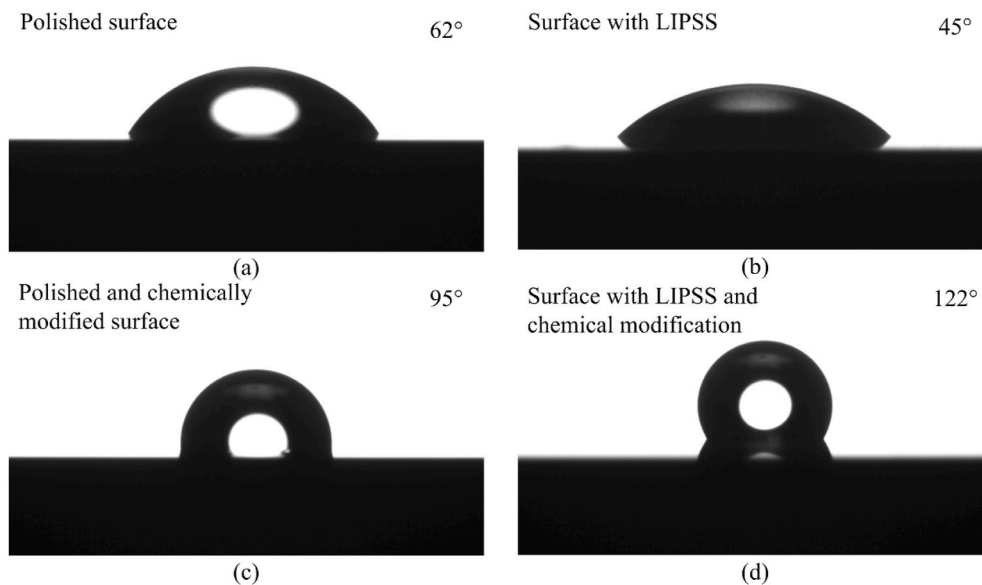


Fig. 14. Contact angles of (a) the polished Ti6Al4V surface, (b) the surface with LIPSS, (c) the polished and then chemically modified surface, and (d) the surface with LIPSS and chemical modification.

SPP could be excited in the molten layer composed of TiN during laser irradiation in nitrogen atmosphere [50,51]. Then, the initial ripples are formed due to the inhomogeneous deposition of laser energy caused by the interference between the incident laser and SPP [52,53], as illustrated in Fig. 12(a). After the initial ripples have been formed, the direct interference between the incident laser and SPP is transformed into the subsequent grating-assisted SPP-laser coupling [40,54], as illustrated in Fig. 12(b). With the action of the grating-assisted SPP-laser coupling, SPP satisfies the phase matching and produces strong resonance, which makes the absorption of laser energy more effective [39,55]. The electric field on the material surface will be redistributed and the enhancement of groove internal field will deepen the groove and finally achieve positive feedback [39,40]. For nanosecond pulse laser, thermal effect is inevitable [46,56]. The melting and evaporation on the material surface will hinder the deepening of grooves, and therefore these ripples are generated under a dynamic equilibrium condition.

5. Potential applications

5.1. Structural coloration

One of the promising applications of LIPSS is to achieve the structural coloration of material surfaces especially the metal surfaces. In this study, effects of the formed LIPSS on the surface color of Ti6Al4V were preliminarily characterized. Fig. 13(a) shows the optical image of the sample after laser irradiation, which includes “nine-squares” and “JLU”. This image was captured in natural light. The size of each square is 3×3 mm, the spacing between two squares is 1 mm, and the size of “JLU” is 5×12 mm. Fig. 13(b) lists the laser parameters corresponding to each square. In Fig. 13(a), the difference in color is observed, and the surface color is changed with the change in laser parameters. When capturing in the relatively dark environment with a vertical light source, the difference of color in the “nine-squares” is evident, as shown in Fig. 13(c). When one of the laser parameters is gradually changed, for example changing the repetition frequency, the surface color shows a transitional tendency, which provides the possibility to control the surface color by changing the laser parameters. Moreover, as shown in Fig. 13(d), when changing the shooting angle, the “JLU” could present various colors. The results in Fig. 13 demonstrate a potential application of the formed LIPSS in coloring of Ti6Al4V surface.

5.2. Wettability

Another important application of LIPSS is to tune the surface wettability of materials. Therefore, the effects of LIPSS on the surface wettability of Ti6Al4V were characterized. Fig. 14 presents the results. Fig. 14(a) shows the contact angle of the polished Ti6Al4V surface, and it is about 62° . The surface with LIPSS generated under selected laser parameters shows a contact angle of 45° , which means that the formed LIPSS slightly increases the hydrophilicity. Fig. 14(c) and (d) show the contact angles of the polished surface and the surface with LIPSS after chemical modification, and the contact angles are 95° and 122° , respectively. The comparative results indicate that the formed LIPSS has changed the wettability of Ti6Al4V surface before or after chemical modification. However, as the formed LIPSS is relatively shallow and the irradiated surface is still quite flat, the change in surface wettability is not obvious.

6. Conclusions

In summary, this study explored the possibility to directly fabricate of LIPSS on the Ti6Al4V surface by nanosecond laser irradiation. By experiments and analysis, the main conclusions could be derived as follows.

- (1) The ripples, a typical LIPSS, could be fabricated on the Ti6Al4V surface by nanosecond laser irradiation in nitrogen atmosphere. Laser irradiation parameters such as the laser power, repetition frequency, and pulse overlap rate significantly affected the morphology of the ripples as well as the surface quality.
- (2) The preferred laser irradiation parameters for fabrication of large-area ripples on Ti6Al4V surface were as follows: $v = 10 \text{ mm s}^{-1}$, $P = 4.46 \text{ W}$, $f = 700 \text{ kHz}$, and $r = 76.6\%$. With these parameters, the formed large-area ripples would be regular and clear, and the final surface quality was better as well.
- (3) Nanosecond laser irradiation in argon atmosphere could not induce the formation of the ripples, demonstrating the assisted role of nitrogen. XRD patterns confirmed the generation of TiN on the surface irradiated in nitrogen atmosphere.
- (4) The formed ripples changed the surface color and wettability of the Ti6Al4V surface.

This study confirms that by nanosecond pulse laser irradiation in nitrogen atmosphere, regular large-area LIPSS could be fabricated on the Ti6Al4V surface, which could achieve surface coloration and tune the surface wettability of Ti6Al4V, thereby accelerating its engineering application as functional materials. In addition, this study may also provide a reference for the preparation of regular LIPSS on the surface of some other alloys by using the nanosecond pulse laser.

Declaration of competing interest

The authors declare that they have no known competing financial interests or personal relationships that could have appeared to influence the work reported in this paper.

Acknowledgements

This work was supported by the National Natural Science Foundation of China (Grant No. 51705197), Science and Technology Project from the Education Department of Jilin Province (Grant No. JJKH20190014KJ), the Graduate Innovation Fund of Jilin University (Grant No. 101832020CX106), and the Fundamental Research Funds for the Central Universities (2019–2021).

References

- [1] Lepicka M, Gradzka-Dahlke M. Surface modification of Ti6Al4V titanium alloy for biomedical applications and its effect on Tribological Properties-A Review. *Rev Adv Mater Sci* 2016;46(1):86–103.
- [2] Elias CN, Lima JHC, Valiev R, Meyers MA. Biomedical applications of titanium and its alloys. *JOM (J Occup Med)* 2008;60(3):46–9.
- [3] Kistler NA, Corbin DJ, Nassar AR, Reutzel EW, Beese AM. Effect of processing conditions on the microstructure, porosity, and mechanical properties of Ti-6Al-4V repair fabricated by directed energy deposition. *J Mater Process Technol* 2019;264:172–81.
- [4] Kundu S, Hussain M, Kumar V, Kumar S, Das AK. Direct metal laser sintering of TiN reinforced Ti6Al4V alloy based metal matrix composite: fabrication and characterization. *Int J Adv Manuf Technol* 2018;97(5–8):2635–46.
- [5] Katahira K, Tanida Y, Takesue S, Komotori J. Rapid surface nitriding of titanium alloy by a nanosecond fiber laser under atmospheric conditions. *CIRP Ann - Manuf Technol* 2018;67(1):563–6.
- [6] Shigematsu I, Nakamura M, Saitou N, Shimojima K. Surface hardening treatments of pure titanium by carbon dioxide laser. *J Mater Sci Lett* 2000;19(11):967–70.
- [7] Seo DM, Hwang TW, Moon YH. Carbonitriding of Ti-6Al-4V alloy via laser irradiation of pure graphite powder in nitrogen environment. *Surf Coating Technol* 2019;363:244–54.
- [8] Fan P, Bai B, Zhong M, Zhang H, Long J, Han J, Wang W, Jin G. General strategy toward dual-scale-controlled metallic micro-nano hybrid structures with ultralow reflectance. *ACS Nano* 2017;11(7):7401–8.
- [9] Wang Q, Samanta A, Toor F, Shaw S, Ding H. Colorizing Ti-6Al-4V surface via high-throughput laser surface nanostructuring. *J Manuf Process* 2019;43:70–5.
- [10] Wang C, Huang H, Qian Y, Zhang Z, Yan J. One-step fabrication of regular hierarchical micro/nano-structures on glassy carbon by nanosecond pulsed laser irradiation. *J Manuf Process* 2021;62:108–18.
- [11] Huang H, Yan JW. Surface patterning of Zr-based metallic glass by laser irradiation induced selective thermoplastic extrusion in nitrogen gas. *J Micromech Microeng* 2017;27(7):075007.

- [12] Guo HY, Li QY, Zhao HP, Zhou K, Feng XQ. Functional map of biological and biomimetic materials with hierarchical surface structures. *RSC Adv* 2015;5(82):66901–26.
- [13] Rotella G, Orazi L, Alfano M, Candamano S, Gnilitkyi I. Innovative high-speed femtosecond laser nano-patterning for improved adhesive bonding of Ti6Al4V titanium alloy. *Cirp J Manuf Sci Tec* 2017;18:101–6.
- [14] Das SK, Andreev A, Messaoudi H, Braenzel J, Schnuerer M, Grunwald R. Highly periodic laser-induced nanostructures on thin Ti and Cu foils for potential application in laser ion acceleration. *J Appl Phys* 2016;119(11):113101.
- [15] Yu Z, Yin S, Zhang WJ, Jiang XQ, Hu J. Picosecond laser texturing on titanium alloy for biomedical implants in cell proliferation and vascularization. *J Biomed Mater Res B* 2019;108:1494–504.
- [16] Kosec T, Legat A, Kovac J, Klobcar D. Influence of laser colour marking on the corrosion properties of low alloyed Ti. *Coatings* 2019;9(6):375.
- [17] Patil D, Aravindan S, Kaushal Wasson M, V P, Rao PV. Fast fabrication of superhydrophobic titanium alloy as antibacterial surface using nanosecond laser texturing. *J Micro Nano-Manuf* 2018;6(1):011002.
- [18] Huerta-Murillo D, García-Girón A, Romano JM, Cardoso JT, Cordovilla F, Walker M, Dimov SS, Ocaña JL. Wettability modification of laser-fabricated hierarchical surface structures in Ti-6Al-4V titanium alloy. *Appl Surf Sci* 2019;463:838–46.
- [19] Florian C, Wonneberger R, Undisz A, Kirner SV, Wasmuth K, Spaltmann D, Krüger J, Bonse J. Chemical effects during the formation of various types of femtosecond laser-generated surface structures on titanium alloy. *Appl Phys A* 2020;126(4).
- [20] Shinonaga T, Tsukamoto M, Kawa T, Chen P, Nagai A, Hanawa T. Formation of periodic nanostructures using a femtosecond laser to control cell spreading on titanium. *Appl Phys B Laser Opt* 2015;119(3):493–6.
- [21] Pan AF, Wang WJ, Mei XS, Wang KD, Yang XB. Rutile TiO₂ flocculent ripples with high antireflectivity and superhydrophobicity on the surface of titanium under 10 ns laser irradiation without focusing. *Langmuir* 2017;33(38):9530–8.
- [22] Sinev DA, Yuzhakova DS, Moskvina MK, Veiko VP. formation of the submicron oxidative LIPSS on thin titanium films during nanosecond laser recording. *Nanomaterials* 2020;10(11).
- [23] Wang Q, Samanta A, Hailu A, Shaw SK, Ding H. Fabrication of mechanically enhanced superhydrophobic surface using nanosecond laser-based high-throughput surface nanostructuring (nHSN). *Procedia CIRP* 2020;87:257–62.
- [24] Huang J, Jiang L, Li XW, Wang AD, Wang Z, Wang QS, Hu J, Qu LT, Cui TH, Lu YF. Fabrication of highly homogeneous and controllable nanogratings on silicon via chemical etching-assisted femtosecond laser modification. *Nanophotonics-Berlin* 2019;8(5):869–78.
- [25] Sun W, Qi H, Fang Z, Yu Z, Yi K, Shao J. 1064nm nanosecond laser induced concentric rings and periodic ripples structures at the exit surface of fused silica. *Appl Surf Sci* 2014;309:79–84.
- [26] Vorobyev AY, Makin VS, Guo C. Periodic ordering of random surface nanostructures induced by femtosecond laser pulses on metals. *J Appl Phys* 2007;101(3):034903.
- [27] Dufft D, Rosenfeld A, Das SK, Grunwald R, Bonse J. Femtosecond laser-induced periodic surface structures revisited: a comparative study on ZnO. *J Appl Phys* 2009;105(3):034908.
- [28] Hu Y, Yao Z. Overlapping rate effect on laser shock processing of 1045 steel by small spots with Nd:YAG pulsed laser. *Surf Coating Technol* 2008;202(8):1517–25.
- [29] Huang H, Yan J. Surface patterning of Zr-based metallic glass by laser irradiation induced selective thermoplastic extrusion in nitrogen gas. *J Micromech Microeng* 2017;27(7):075007.
- [30] Thijs L, Verhaeghe F, Craeghs T, Humbeek JV, Kruth J-P. A study of the microstructural evolution during selective laser melting of Ti-6Al-4V. *Acta Mater* 2010;58(9):3303–12.
- [31] Zhao ZY, Li L, Bai PK, Jin Y, Wu LY, Li J, Guan RG, Qu HQ. The heat treatment influence on the microstructure and hardness of TC4 titanium alloy manufactured via selective laser melting. *Materials* 2018;11(8):1318.
- [32] Simonelli M, Tse YY, Tuck C. On the texture formation of selective laser melted Ti-6Al-4V. *Metall Mater Trans* 2014;45(6):2863–72.
- [33] Birnbaum M. Semiconductor surface damage produced by ruby lasers. *J Appl Phys* 1965;36(11):3688–9.
- [34] Ran L, Guo Z, Qu S. Self-organized periodic surface structures on ZnO induced by femtosecond laser. *Appl Phys A* 2010;100(2):517–21.
- [35] Bonse J, Krüger J, Höhm S, Rosenfeld A. Femtosecond laser-induced periodic surface structures. *J Laser Appl* 2012;24(4):065006.
- [36] Wang J, Guo C. Ultrafast dynamics of femtosecond laser-induced periodic surface pattern formation on metals. *Appl Phys Lett* 2005;87(25):251914.
- [37] Rajab FH, Tariq AST, Al-Jumaily AK, AlShaer AW, Li L, Whitehead KA. The influence of picosecond laser generated periodic structures on bacterial behaviour. *Appl Surf Sci* 2021;540:148292.
- [38] Sanz M, Rebollar E, Ganeev RA, Castillejo M. Nanosecond laser-induced periodic surface structures on wide band-gap semiconductors. *Appl Surf Sci* 2013;278:325–9.
- [39] Xia Z, Chen C, Fang H, Chen S. The mechanism and process of nanosecond pulsed-laser induced subwavelength periodic ripples on silica films. *Appl Surf Sci* 2015;337:151–7.
- [40] Huang M, Zhao FL, Cheng Y, Xu NS, Xu ZZ. Origin of laser-induced near-subwavelength ripples: interference between surface plasmons and incident laser. *ACS Nano* 2009;3(12):4062–70.
- [41] Kobayashi T, Sera H, Wakabayashi T, Endo H, Takushima Y, Yan J. Surface flattening and nanostructuring of steel by picosecond pulsed laser irradiation. *Nanomanufacturing and Metrology* 2018;1(4):217–24.
- [42] Kobayashi T, Wakabayashi T, Takushima Y, Yan J. Formation behavior of laser-induced periodic surface structures on stainless tool steel in various media. *Precis Eng* 2019;57:244–52.
- [43] Peng LP, Yan DW, Wang XM, Wang YY, Liu HN, Wu WD. Self-organized subwavelength ripple by nanosecond laser induced chemical vapor deposition. *Thin Solid Films* 2014;567:87–90.
- [44] Ehrhardt M, Han B, Frost F, Lorenz P, Zimmer K. Generation of laser-induced periodic surface structures (LIPSS) in fused silica by single NIR nanosecond laser pulse irradiation in confinement. *Appl Surf Sci* 2019;470:56–62.
- [45] Lai S, Lorenz P, Ehrhardt M, Han B, Hirsch D, Zagoranskiy I, Lu J, Zimmer K. Laser-induced frontside etching of silicon using 1550-nm nanosecond laser pulses. *Opt Laser Eng* 2019;122:245–53.
- [46] Xia Z, Li D, Zhao Y a, Wu Y. New damage behavior induced by nanosecond laser pulses on the surface of silica films. *Opt Laser Eng* 2013;46:77–80.
- [47] Derrien TJ, Krüger J, Bonse J. Properties of surface plasmon polaritons on lossy materials: lifetimes, periods and excitation conditions. *J Optics-Uk* 2016;18(11):115007.
- [48] Pflüger J, Fink J, Weber W, Bohnen KP, Crecelius G. Dielectric properties of TiCx, TiNx, VCx, and VNx from 1.5 to 40 eV determined by electron-energy-loss spectroscopy. *Phys Rev B* 1984;30(3):1155–63.
- [49] Bonse J, Hohm S, Kirner SV, Rosenfeld A, Krüger J. Laser-induced periodic surface structures— a scientific evergreen. *IEEE J Sel Top Quant* 2017;23(3):9000615.
- [50] Satapath Pravarakar, Panda Rudrashish, Sahoo Rajashree, Shukla Mukesh Kumar, Khatua Lizina, , Pratap Kumar Sahoo, Das R, Das SK. Observation of continuous and non-continuous laser induced periodic structures on silicon. *J Laser Micro Nanoen* 2018;13(3):146–9.
- [51] Bonse J, Munz M, Sturm H. Structure formation on the surface of indium phosphide irradiated by femtosecond laser pulses. *J Appl Phys* 2005;97(1):013538.
- [52] Hong L, Rusli, Wang XC, Zheng HY, Wang H, Yu HY. Femtosecond laser fabrication of large-area periodic surface ripple structure on Si substrate. *Appl Surf Sci* 2014;297:134–8.
- [53] Barnes WL, Dereux A, Ebbesen TW. Surface plasmon subwavelength optics. *Nature* 2003;424:824–30.
- [54] Zou T, Zhao B, Xin W, Wang Y, Wang B, Zheng X, Xie H, Zhang Z, Yang J, Guo CL. High-speed femtosecond laser plasmonic lithography and reduction of graphene oxide for anisotropic photoresponse. *Light Sci Appl* 2020;9:69.
- [55] Liu W, Jiang L, Han W, Hu J, Li X, Huang J, Zhan S, Lu Y. Manipulation of LIPSS orientation on silicon surfaces using orthogonally polarized femtosecond laser double-pulse trains. *Opt Express* 2019;27(7):9782–93.
- [56] Nürnberger P, Reinhardt HM, Kim H-C, Pfeifer E, Kroll M, Müller S, Yang F, Hampf NA. Orthogonally superimposed laser-induced periodic surface structures (LIPSS) upon nanosecond laser pulse irradiation of SiO₂/Si layered systems. *Appl Surf Sci* 2017;425:682–8.